Electron collisions with the CF radicals using the *R*-matrix method

INSTITUTE OF PHYSICS PUBLISHING JOURNAL OF PHYSICS B: ATOMIC, MOLECULAR AND OPTICAL PHYSICS

J. Phys. B: At. Mol. Opt. Phys. **36** (2003) 2419–2432 PII: S0953-4075(03)61087-4

Electron collisions with the CF radicals using the *R*-matrix method

I Rozum[1], **N J Mason**[2] **and Jonathan Tennyson**[1]

[1] Department of Physics and Astronomy, University College London, Gower Street, London WC1E 6BT, UK
[2] Centre of Molecular and Optical Sciences, The Open University, Milton Keynes, UK

Received 18 March 2003
Published 30 May 2003
Online at stacks.iop.org/JPhysB/36/2419

Abstract

The *R*-matrix method is used to treat electron collisions with the diatomic radical CF as a function of internuclear separation, R. These calculations concentrate on obtaining low-energy (<10 eV) elastic and excitation cross sections of the five lowest-lying electronically excited states of the symmetries $X\,^2\Pi$, $^4\Sigma^-$, $^2\Sigma^+$, $^2\Delta$, $^2\Sigma^-$ and $^4\Pi$, with vertical excitation energies in the range of 2.86–10 eV. Special measures are required to treat $^2\Sigma^+$, which is Rydberg-like for $R < 2.6\ a_0$. Three shape resonances of $^3\Sigma^-$, $^1\Delta$ and $^1\Sigma^+$ symmetries are fitted. The $^1\Delta$ and $^1\Sigma^+$ resonances have a position of 0.91 and 2.19 eV respectively at the equilibrium bond length of CF. The position of the $^3\Sigma^-$ resonance is close to zero at $R_e = 2.44\ a_0$ and the resonance becomes bound at larger R. Two weakly bound states of symmetries $^3\Pi$ and $^1\Pi$ were also detected at the equilibrium geometry. Calculations which stretch the C–F bond show that the $^1\Delta$ resonance becomes bound at $R = 3.3\ a_0$ and $^1\Sigma^+$ at larger R.

(Some figures in this article are in colour only in the electronic version)

1. Introduction

Low-temperature plasmas play a key role in the modern semiconductor, materials and lighting industries and are used to process everything from computer chips to aircraft components. Therefore, plasma etching technology has become one of the leading commercial industries with a global turnover of in excess of one billion dollars. However, despite its high cost and technical importance, plasma equipment is still largely designed empirically, with little help from computer simulations. The high cost of developing the new plasma equipment and optimizing plasma reactor organization has motivated the development of large-scale modelling and simulations. However, the major roadblock to the development of such a strategy is the lack of a definitive database for many chemical and physical processes that occur in the plasma, in particular knowledge of the underlying collision processes.

Perfluorinated gases (PFCs) currently used in plasma processing have been found to be detrimental to the environment and global climate. PFCs, which are only partially consumed in the etch process, are emitted into the atmosphere. They have an extremely high global warming potential (up to four orders of magnitude higher than CO_2) and atmospheric lifetimes (>1000 years) that are practically infinite on the time scale of human development. Recent emission reduction strategies, as prescribed by the Kyoto protocol, have to combine both optimization of plasma equipment efficiency and the search for new plasma compounds. CF_3I and C_2F_4 have been proposed as new plasma reactants (Samukawa *et al* 1999). They both have a low global warming potential and under electron bombardment provide a strong source of CF, CF_2 and CF_3 radicals (Mason *et al* 2003) for etching of silicon surfaces. Knowledge of collision processes with CF_x radicals is, therefore, required. However, CF_x radicals are highly reactive and are therefore difficult molecules to work with in the laboratory, requiring the development of *ab initio* methods to estimate collision cross sections. The results of our calculations on CF_2 have already been published (Rozum *et al* 2002). In this work we investigate electron collisions with the diatomic radical CF using the UK *R*-matrix method (Morgan *et al* 1998).

2. Theoretical approach

The *R*-matrix method is based on the splitting of coordinate space into two regions by a spherical boundary of radius $r = a$ centred on the centre of mass of the molecule: the inner region and the outer region (Burke and Berrington 1993, Morgan *et al* 1998). The boundary is placed so that the inner region contains the electronic charge cloud of the target molecule. The interaction between the electron and the target molecule has different features in the inner region and outer region. Inside the *R*-matrix sphere the scattering electron lies within the molecular charge cloud and exchange and electron–electron correlation must be taken into account. Quantum chemistry methods can be adopted to find the wavefunction in this region. In the outer region exchange and correlation are assumed to be negligible and only long-range multipolar interactions between the scattering electron and the target are included. Thus it is possible to reduce the scattering problem in the external region to the solution of a set of coupled, ordinary differential equations.

In the inner region the total wavefunction describing scattering of an electron by an *N*-electron molecule can be expanded as (Burke and Berrington 1993)

$$\Psi_k^{N+1} = A \sum_I \psi_I^N(x_1, \ldots, x_N) \sum_j \xi_j(x_{N+1}) a_{Ijk} + \sum_m \chi_m(x_1, \ldots, x_N, x_{N+1}) b_{mk} \tag{1}$$

where A is the antisymmetrization operator, x_n is the spatial and spin coordinate of the nth electron, ξ_j is a continuum orbital spin-coupled with the scattering electron and a_{Ijk} and b_{mk} are variational coefficients determined by our program. The first summation runs over all CI target states and gives terms known as 'target + continuum' configurations. The second summation runs over configurations χ_m, where all electrons are placed in target molecular orbitals. These configurations are generally described as square integrable.

The general application of the *R*-matrix method to polyatomic molecules employing the UK polyatomic *R*-matrix code has been described in the literature (Morgan *et al* 1998, Tennyson and Morgan 1999). The application of these codes to electron collisions with Cl_xO_y radicals was described by Baluja *et al* (2000, 2001a, 2001b).

Table 1. CF basis set.

Carbon[a]			Fluorine[b]		
n	l	ζ	n	l	ζ
1	0	9.25	1	0	7.943 74
1	0	5.54	1	0	14.109 46
2	0	5.31	2	0	1.934 65
2	0	2.04	2	0	3.256 33
2	0	1.31	3	0	9.925 40
2	1	6.53	2	1	1.407 01
2	1	2.61	2	1	2.373 25
2	1	1.44	2	1	4.278 43
2	1	0.96	2	1	8.972 51
3	2	2.35	3	2	1.835 39
3	2	1.24	3	2	3.367 96
4	3	2.35	4	3	2.700 10

[a] From Cooper and Kirby (1987).
[b] From McLean and Yoshimine (1967).

2.1. Target representation

The CF radical was first observed spectroscopically by Andrews and Barrow in 1950 and has since been the subject of considerable experimental and theoretical interest. In more recent times, it has been identified as an important species in fluorocarbon plasmas.

The equilibrium geometry of CF was derived from analysis of its emission spectrum (Porter *et al* 1965, Carroll and Grennan 1970). According to these studies the C–F bond length is 2.44 a_0 at equilibrium. *Ab initio* calculations on geometry of CF, performed at multireference configuration interaction (MRCI) level (Hess and Buenker 1986, Rendell *et al* 1989) are in good agreement with the experimental values and between themselves.

Several studies of the low-lying states of CF have been reported in the literature (Dunning *et al* 1979, Hall and Richards 1972, Huber *et al* 1979, Grieman *et al* 1983, Petsalakis 1999). The low-lying valence states of CF were studied in detail by Dunning *et al* (1979) and by Petsalakis (1999) using the MRCI method. Petsalakis also performed detailed studies of Rydberg states of CF and generated potential energy curves using quantum defect calculations.

The ground state dipole moment of the CF radical estimated from Stark effects by Saito *et al* (1983) is 0.645 ± 0.014 D(1 D = 0.3937 au). This result agrees with the value 0.65 ± 0.05 D obtained by Carrington and Howard (1970) and by Byfleet *et al* (1971).

Our inner region target calculations have been carried out on the six states of CF which are $X\,^2\Pi$, $^4\Sigma^-$, $^2\Sigma^+$, $^2\Delta$, $^2\Sigma^-$ and $^4\Pi$. We used an equilibrium value for a C–F bond length $R_e = 2.44\ a_0$. The basis set of Slater type functions consisted of 24σ and 14π functions equally distributed on the two nuclei (table 1). In order to describe the Rydberg state $B\,^2\Sigma^+$, the basis set was supplemented with up to two σ and two π functions with diffuse exponents on each atom, which are called 'Rydberg basis functions' below. Although, the excited states 2–4 $^2\Sigma^+$, 2 $^2\Delta$, 3 $^2\Delta$ and 2–5 $^2\Pi$ have vertical excitation energies below 10 eV (Petsalakis 1999), we do not include these states in our calculations because they are Rydberg-like and require a large number of diffuse orbitals. It is numerically and computationally impractical to include large numbers of diffuse orbitals (i.e. those with very small exponents) as they will require a very large *R*-matrix sphere. Neglecting Rydberg states can result in unphysical pseudo-resonances at collision energies above about 5 eV; the exact energy is geometry-dependent.

Table 2. Exponents for the Rydberg basis functions 3s and 3pσ on C and F atoms.

	Orbitals on carbon		Orbitals on fluorine	
Basis	3s	3pσ	3s	3pσ
A	0.5856, 0.30	0.4855, 0.24	1.77, 0.73	1.48, 0.54
B	0.5856, 0.40	0.4855, 0.30	1.77, 0.73	1.48, 0.54
C	0.5856, 0.44	0.4855, 0.38	1.77, 0.73	1.48, 0.54
D	0.5856	0.4855	1.77	1.48

The target calculations consisted of two parts. Valence state-averaged natural orbitals (NO), obtained from 'all singles and doubles' configuration interaction (CI) calculations for all six target states, were used for treating valence target states. The number of configurations, used to build valence NOs, is 103 124 for the ground state, 46 124 for the quartet symmetry and around 65 000 for each state of doublet symmetry. The Rydberg Slater-type basis functions were not included at this stage of the calculations. For a description of the Rydberg state $^2\Sigma^+$ it was necessary to include Rydberg molecular orbitals in the wavefunctions. Rydberg molecular orbitals were obtained from Rydberg NO for Σ symmetry, following the prescription of Cooper and Kirby (1987). They were constructed from single-excitation CI calculations of the order 31 088 configurations, with all possible arrangements of ten valence electrons and one electron excited into a separate Rydberg orbital space (7σ–$14\sigma\,3\pi$–6π) (Cooper and Kirby 1987). In final target calculations we partitioned the molecular orbitals into three spaces: core orbitals ($1\sigma\,2\sigma$), valence orbitals ($3\sigma\ldots6\sigma\,1\pi\,2\pi$) and Rydberg orbitals ($7\sigma\,3\pi$). The valence state-averaged NO were used to calculate core and valence molecular orbitals. For calculation of Rydberg molecular orbitals we used Rydberg NO, Schmidt orthogonalized to the other target orbitals. Our final complete active space configuration interaction (CASCI) model, therefore, consisted of two types of configuration:

$$(1\sigma\,2\sigma)^4(3\sigma\ldots6\sigma\,1\pi\,2\pi)^{11}$$

and

$$(1\sigma\,2\sigma)^4(3\sigma\ldots6\sigma\,1\pi\,2\pi)^{10}(7\sigma\,3\pi)^1.$$

Considerable care must be taken when choosing the Rydberg orbital space. Too many diffuse orbitals can lead to problems with linear dependence in the N-electron target calculations and even more severe problems in the $(N+1)$ scattering calculations.

Several basis sets with different exponents for the Rydberg basis functions 3s and 3pσ on the C atom were tested in the course of this work (table 2). Basis B did not give good vertical excitation energies. Target properties obtained using basis functions A and C are in a good agreement with the experimental and theoretical data at equilibrium geometry. At non-equilibrium geometries basis C gives a severe linear dependence for $R < 2.0\,a_0$ and basis A gives a strong orbital crossing at $R = 2.7\,a_0$, which could not be removed. Finally we chose the basis D with four added Rydberg basis functions as this model gave us the most stable results at different R-matrix radii and satisfactory excitation energies.

Table 3 compares the vertical excitation energies for the states considered in our calculation with data available in the literature. Our CASCI model gives a ground state dipole moment of 0.64 D. This value is in very good agreement with the experimental value of Saito *et al* (1983) 0.645 ± 0.014 D.

For the calculation of target properties at non-equilibrium geometry we used the same model as the one described for equilibrium geometry. The electronic state energies as a function of changing C–F bond length are plotted in figure 1. The profiles of the energy

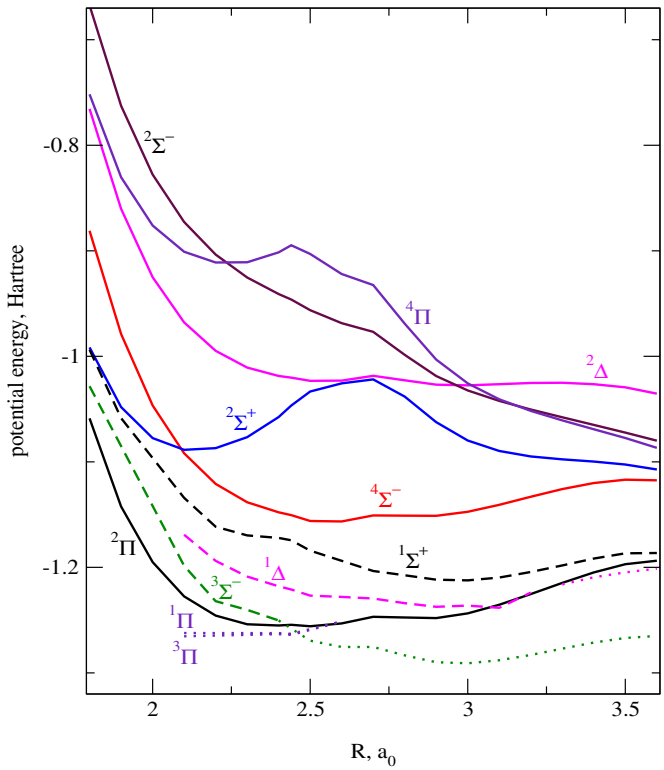

Figure 1. Electronic state energies of CF as a function of changing C–F bond length (R), solid curves. The dashed curves represent the CF resonance energy curves; the dotted curves below the ground state curve represent the CF bound state curves. −136.00 should be added to the energy entries.

Table 3. Excitation energies Δ (in eV) for the CF target states generated using our model at equilibrium geometry. Also given are the dominant configuration of each state and the number of configurations N in our calculations. The absolute energy E (in Hartree) of the ground state is also given.

		This work			Theory	Observed
State	Dominant configuration	N	Δ	E	Δ	Δ
$X\,^2\Pi$	$1\sigma^2 \ldots 5\sigma^2 1\pi^2 2\pi$	1786	0	−137.2544	0	0
$^4\Sigma^-$	$5\sigma^{-1}2\pi$	797	2.83		2.9[a]/2.66[b]	—
$^2\Sigma^+$	$2\pi^{-1}6\sigma$	1072	5.65		5.65[c]	5.293[d]
$^2\Delta$	$5\sigma^{-1}2\pi$	1100	6.37		6.36[c]	6.125[d]
$^2\Sigma^-$	$2\pi^{-1}6\sigma$	1016	8.39		7.96[c]	—
$^4\Pi$	$5\sigma^{-1}6\sigma$	1269	9.79		—	—

[a] From Hall and Richards (1972).
[b] From Dunning *et al* (1979).
[c] From Petsalakis (1999).
[d] From Huber *et al* (1979).

curves for the states $X\,^2\Pi$, $^2\Sigma^+$, $^2\Delta$ and $^2\Sigma^-$ are in agreement with the results of Petsalakis (1999, figures 1, 2), who studied all the doublet electronic states of CF using MRCI calculations. The $^4\Sigma^-$ state energy curve is generally comparable with the potential energy curve for the

same state derived from *ab initio* calculations by Luque *et al* (2003, figure 1). There are no data on the absolute and excitation energies for the $^4\Pi$ state of CF available in the literature.

At bond lengths below 2.6 a_0 the potential energy curve of the excited Rydberg state $^2\Sigma^+$ follows the ground state potential energy curve of CF^+ and has a Rydberg-like shape (see Petsalakis 1999, figure 1). However, the character of this state changes from Rydberg to valence at a C–F bond length of 2.6 a_0. This can be explained by considering the second $^2\Sigma^+$ Rydberg state, not included in our calculations. The first $^2\Sigma^+$ state is characterized by a single configuration, with an open shell in the 6σ orbital, which has Rydberg s character at bond lengths below 2.6 a_0. At larger bond lengths 6σ passes the Rydberg s character to the next σ orbital, which has Rydberg p character at shorter bonds, and takes the valence character. Therefore, the shape of the Rydberg $^2\Sigma^+$ state energy curve results from an avoided crossing with the second Rydberg $^2\Sigma^+$ state (see Petsalakis 1999). The $^2\Delta$ potential energy curve has a weak maximum at a bond length around 3.5 a_0. This is a result of an avoided crossing with the second repulsive $^2\Delta$ state (Petsalakis 1999, figure 2). We note that the $^4\Pi$ potential energy curve also has a double well structure. From the analysis of the CF potential energy curves, the $^4\Pi$ state shows a behaviour similar to that of the Rydberg $^2\Sigma^+$ state and may also be Rydberg-like. The shape of the $^4\Pi$ potential energy curve at $R \sim 2.5\ a_0$ probably results from an avoided crossing.

Our potential energy curves (figure 1) show a weak structure at a bond length of 2.7 a_0 for most of the states of CF. This structure is caused by a crossing of 6σ and 7σ orbitals in the orbital set, which we were unable to remove.

2.2. Scattering model

Our final calculations used the six states given in table 3. Since CF is an open shell radical with the ground state $X\,^2\Pi$, two spin-specific scattering symmetries, singlet and triplet, are considered in this study.

Test calculations for several R-matrix radii ($a = 10\ a_0$, 12 a_0 and 13 a_0) were performed to test the stability of our model and assign the resonances. The R-matrix radius 10 a_0 is too small for our calculations. This caused weak linear dependence in the $(N + 1)$ calculations in almost all of the states of CF that was partially cured by removing one π orbital using Lagrange orthogonalization (Tennyson *et al* 1987). With 10 a_0 all our results showed significant unphysical structure which we attributed to the target wavefunctions leaking outside the R-matrix sphere. Tests using $a = 12\ a_0$ and 13 a_0 showed that the structure largely disappeared. Our calculations show strong dependence of the excitation cross section $X\,^2\Pi \rightarrow {}^2\Sigma^+$ on the R-matrix radius (figure 2). All other cross sections are much less dependent upon the R-matrix radius. Our final calculations used the R-matrix radius of 13 a_0 and propagation to a radius of 80.1 a_0, as this model did not give us any linear dependence.

In all calculations, the continuum basis functions were represented by numerical orbitals of up to $l \leqslant 6$ partial waves, centred on the centre of gravity of the molecule. At $a = 13\ a_0$ the continuum orbitals consisted of $82\sigma, 69\pi$ and 56δ orbitals that were orthogonalized to the target orbitals using only Schmidt orthogonalization (Tennyson *et al* 1987). The $(N + 1)$ electron calculations must use a model which balances that of the CF target. The 'L^2' configurations χ_m in (1) are constructed from the target orbitals and contain the incident and target electrons placed in the target molecular orbitals. In this work the square integrable term consists of two types of configuration that allow for the relaxation of the orthogonality between the target valence, Rydberg and continuum orbitals:

$$(1\sigma 2\sigma)^4(3\sigma \ldots 6\sigma 1\pi 2\pi)^{12}$$

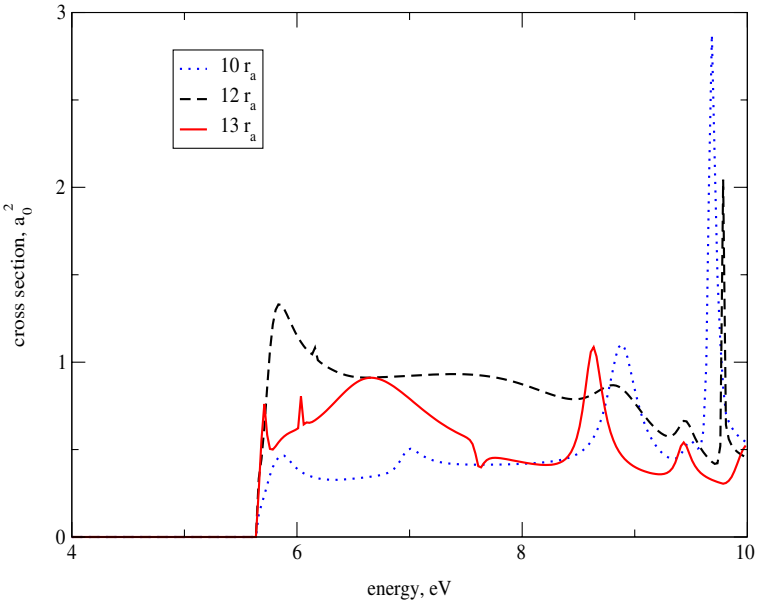

Figure 2. Total cross sections for electron impact excitation of the second excited Rydberg state $^2\Sigma^+$ plotted at different R-matrix radii.

and

$$(1\sigma 2\sigma)^4(3\sigma \ldots 6\sigma 1\pi 2\pi)^{11}(7\sigma 3\pi)^1.$$

CF is a polar molecule and the elastic scattering cross section of a static molecule with a permanent dipole moment is divergent. A very large number of partial waves and rotational effects must be included in order to obtain convergent results. States with $l > 6$ omitted from our calculations were added using a Born correction (Chu and Dalgarno 1974). The Born correction depends on target properties and a number of partial waves included in the expansion of the scattering amplitude but does not depend on the radius of the R-matrix sphere. Our tests showed that the maximum effect from using a Born correction was for the excitation to $^2\Sigma^+$ and $^2\Delta$ states at short bond lengths.

The range of scattering energies was restricted to energies below 10 eV. Resonance positions and widths were found by fitting the eigenphase sum to a Breit–Wigner profile, using the RESON program (Tennyson and Noble 1984). Particular emphasis was given to resonances in the energy range below 5 eV, as this is the typical energy of etching plasmas. In order to study the dissociative behaviour of resonances we performed calculations in which the C–F bond was stretched from $R = 1.8\ a_0$ to $3.6\ a_0$.

3. Results

3.1. Elastic scattering

Elastic cross sections for the electron scattering off the CF radical were calculated at different geometries. Previous R-matrix calculations show disagreement between Born-corrected cross sections and the experimental values at energies below 100 meV, as the calculated cross sections do not reproduce the sharp minimum observed in the experiments (see for example Baluja *et al* 2001a). According to Field *et al* (2000), this structure is due to interference effects between

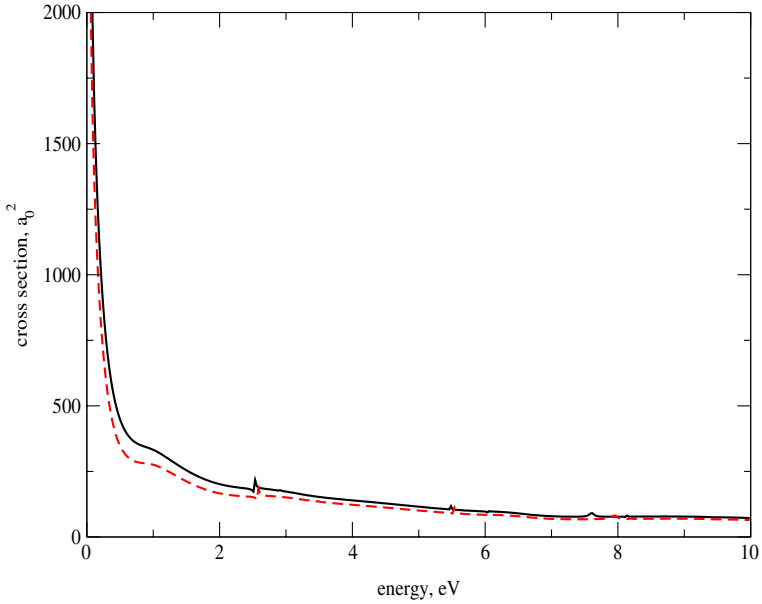

Figure 3. Total elastic cross section for the CF molecule at equilibrium geometry. The dashed curve represents the cross section without a Born correction. The solid curve represents the cross section with an added Born correction.

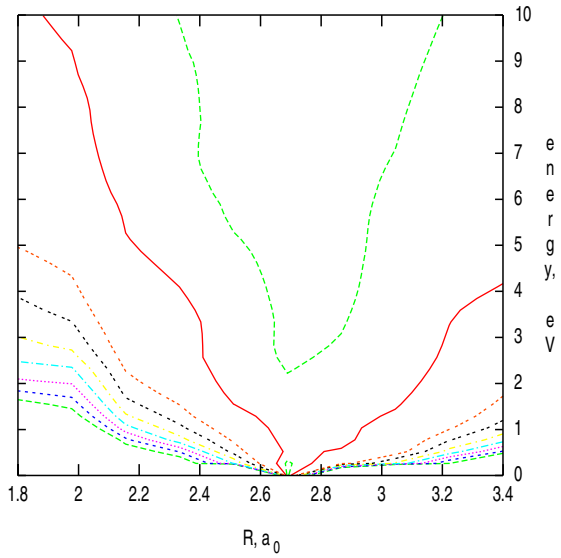

Figure 4. Total elastic cross sections for the CF molecule plotted at different C–F bond lengths, R. Contours range from 90 a_0^2 (top contour) to 900 a_0^2 (bottom curve) in steps of 90 a_0^2.

rotational (and other) channels. Our model does not include rotational coupling, and therefore will not be reliable at these ultra low energies.

The resulting elastic cross sections for CF summed over all singlet and triplet symmetries for our six-state model are shown in figure 3. It can be seen that the Born correction for the

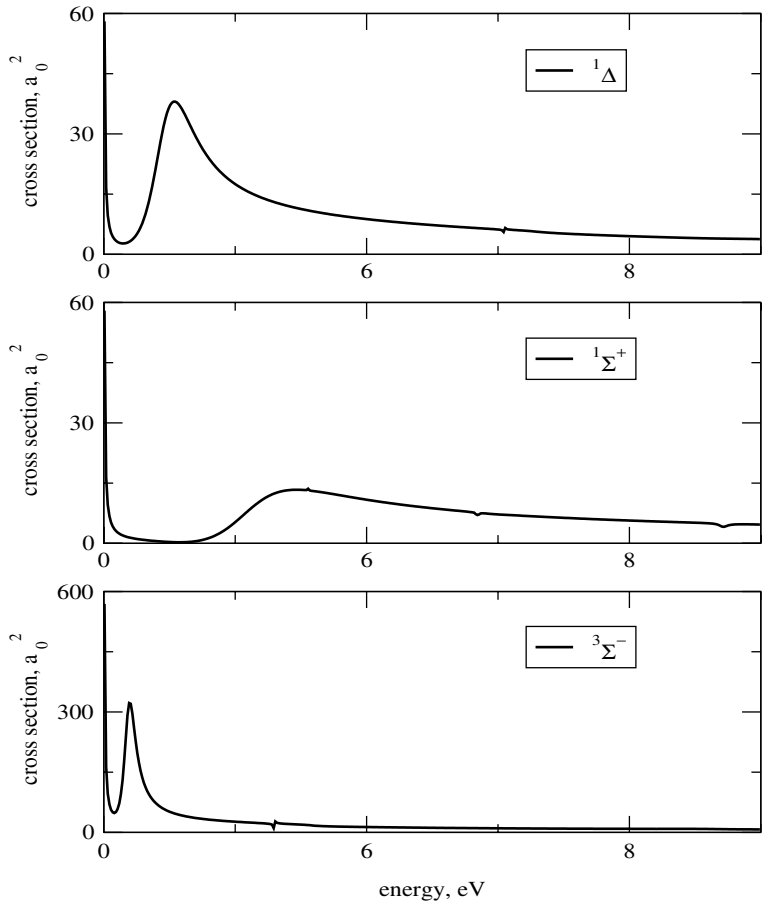

Figure 5. The top and middle graphs present $^1\Delta$ and $^1\Sigma^+$ contributions respectively to the total elastic cross section, plotted at the equilibrium geometry of CF. The bottom graph presents the $^3\Sigma^-$ contribution to the total elastic cross section plotted at the C–F bond length 2.3 a_0. All the graphs illustrate shape resonances.

elastic cross section at the equilibrium geometry of the CF is small. Figure 4 gives the contour plot of the Born corrected elastic cross sections at different bond lengths.

The main feature in the elastic cross section is a presence of three prominent resonances of symmetries $^1\Delta$, $^1\Sigma^+$ and $^3\Sigma^-$ (figure 5). At equilibrium geometry the $^1\Delta$ resonance has a position and width of 0.91 and 0.75 eV respectively. The corresponding parameters for the $^1\Sigma^+$ resonance are 2.19 and 1.73 eV. We could not determine the position of the $^3\Sigma^-$ resonance at equilibrium geometry as it is very close to zero energy and the resonance is about to become bound. This will be discussed in the next subsection. The energies of these resonances as a function of a bond length are plotted in figure 1 and their widths in figure 6. As can be seen from the figure 6, the $^3\Sigma^-$ resonance narrows rapidly with increasing R. The structure in the resonance widths of $^1\Sigma^+$ and $^1\Delta$ symmetries below 2.4 a_0 may be caused by crossings of the potential energy curves (figure 1). The $^3\Sigma^-$, $^1\Delta$ and $^1\Sigma^+$ resonances are shape resonances with the same dominant configuration $2\pi^2$.

Figure 4 shows the magnitude of the total elastic cross section as a function of the C–F bond length. It decreases as R increases from 1.8 to 2.7 a_0 and has a minimum about $R = 2.7$ a_0,

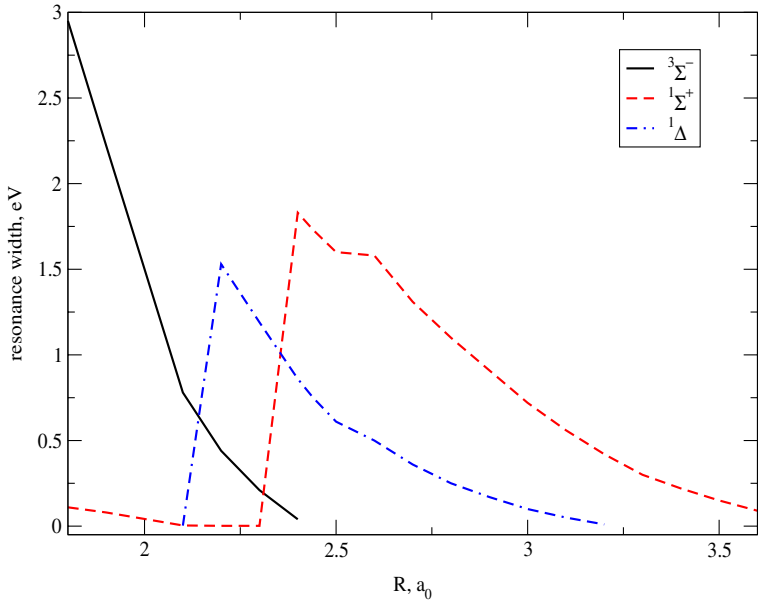

Figure 6. Resonance width as a function of C–F bond length. The solid curve represents a width of the shape resonance of $^3\Sigma^-$ symmetry. Dashed and dot–dashed curves represent a width of the shape resonances of $^1\Sigma^+$ and $^1\Delta$ symmetries respectively.

where the ground state dipole moment changes sign. With a further increase of the CF bond from 2.8 to 3.4 a_0 the magnitude of the total elastic cross section increases.

3.2. Bound states

The energy of the bound states was calculated from the scattering wavefunctions using the program BOUND (Sarpal *et al* 1991). Our calculations show the presence of two weakly bound states of symmetries $^1\Pi$ and $^3\Pi$ for $R < 2.6\ a_0$ with binding energy of 0.23 and 0.26 eV respectively at equilibrium. These bound states are very diffuse and have only 0.2 and 1% of their wavefunctions respectively in the R-matrix box at equilibrium, which makes it difficult to determine their energies accurately. These states are largely dipole bound and are, therefore, sensitive to the value of the target dipole moment. At $R = 2.6\ a_0$ the ground state dipole moment of CF is near zero and the $^1\Pi$ and $^3\Pi$ bound states become unbound and create two resonances with positions 0.054 eV for $^1\Pi$ and 0.050 eV for $^3\Pi$ symmetries. These are shape resonances with the same configuration $2\pi 7\sigma$. We could not detect these resonances for $R > 2.7\ a_0$. The $^1\Pi$ and $^3\Pi$ bound states may become unbound in the whole range of R if rotational motion is taken into account.

With increasing C–F bond length the $^3\Sigma^-$ and $^1\Delta$ resonance energy curves approach the ground state energy curve. At $R = 2.5\ a_0$, the $^3\Sigma^-$ resonance becomes bound (see figure 1). This bound state has 99% of the wavefunction inside the R-matrix sphere. For $R > 3.3\ a_0$ the $^1\Delta$ resonance also becomes bound. The energies of these bound states are plotted in figure 1. The resonance parameters suggest that the $^1\Sigma^+$ resonance will also become bound, but only at bond lengths larger than those considered here. The $^3\Sigma^-$, $^1\Delta$ and $^1\Sigma^+$ resonances thus display the classic behaviour one would expect of resonances supporting dissociative attachment (DA). Asymptotically the $^3\Sigma^-$ and $^3\Pi$ states dissociate to $C(^3P) + F^-(^1S)$, as the

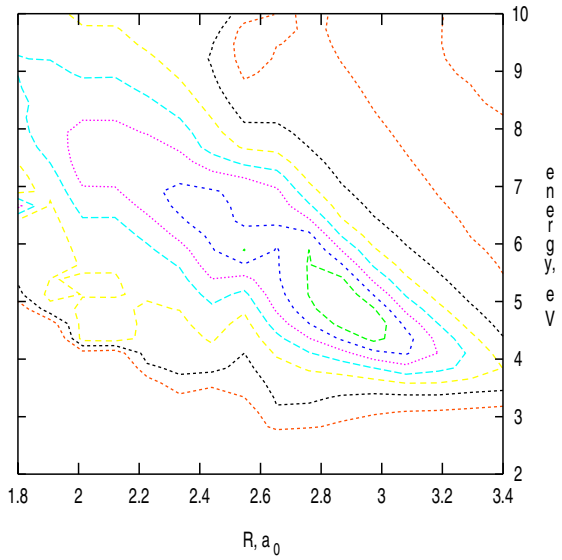

Figure 7. Contour plot of total cross sections for electron impact excitation of the lowest excited $^4\Sigma^-$ state of CF plotted as a function of bond length, R. Contours range from 0.4 a_0^2 (bottom curve) to 3.2 a_0^2 (innermost closed contour) in steps of 0.4 a_0^2.

electronic affinity of F is higher than the affinity of C, while $^1\Sigma^+$, $^1\Pi$ and $^1\Delta$ correlate with the excited $C(^1D) + F^-(^1S)$.

The equilibrium magnitude of the total elastic cross section is 6000 a_0^2 at a scattering electron energy of 100 meV. The magnitude of DA cross sections is generally high, typically 10% of the total scattering cross section. We might expect CF to have a DA cross section of this magnitude.

3.3. Inelastic scattering

Figure 7 presents the electron-impact electronic excitation cross section from the ground $X\,^2\Pi$ state to the first excited metastable $^4\Sigma^-$ state. This spin-changing transition is dipole forbidden. The resonance features in the energy region 7–9 eV are unphysical due to the neglect of some Rydberg excited states with the excitation energies in this region.

Transitions from the ground $X\,^2\Pi$ state to the second, third and fourth excited states are dipole allowed. The cross section for the transition into the $^2\Sigma^+$ Rydberg state is shown in figure 8. The cross section is rich in resonance features in the energy region above 5 eV, most of which are, probably, pseudo-resonances. The double minimum nature of the $^2\Sigma^+$ state means that as R increases from 1.8 a_0 the threshold initially increases, then decreases from $R = 2.6\ a_0$. The structure of the cross section for excitation to the Rydberg-like $^2\Sigma^+$ state, at small R, differs significantly from that for excitation to the valence $^2\Sigma^+$ state, at larger R. This is shown by the unusual shape of the contours in figure 8, which show a minimum in the cross section at around $R = 2.6\ a_0$. We anticipate that inclusion of vibrational effects would give a somewhat unusual dependence on vibrational quantum numbers for this cross section.

Figure 9 presents the Born corrected cross section for the transition into the third excited state $^2\Delta$. The Born correction is significant at incident electron energies above 8 eV and increases with the increasing R. There are no resonance features apparent in this excitation cross section.

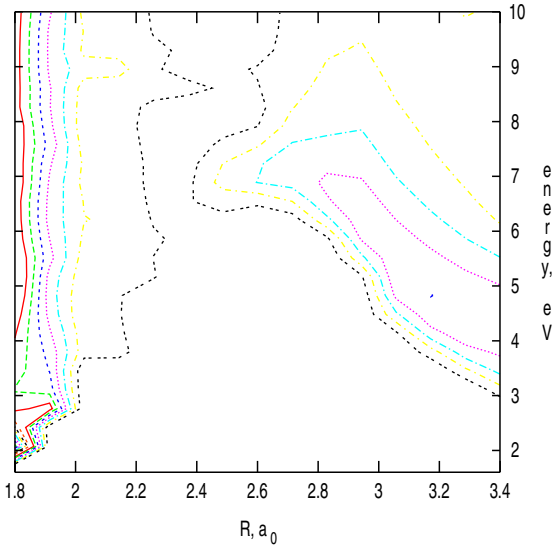

Figure 8. Contour plot of total cross sections, including Born correction, for electron impact excitation of the second excited $^2\Sigma^+$ state, plotted as a function of C–F bond length R. The cross section for this process is small for intermediate bond lengths ($R \approx 2.5\ a_0$). Contours start at $0.8\ a_0^2$ from this region and increase in steps of $0.8\ a_0^2$ to a maximum of $4.0\ a_0^2$ (at $R = 3.2\ a_0$ and $E = 4.8$ eV) at large R. At small R the cross section shows a strong peak at low energy rising to above $12\ a_0^2$ (at $R = 1.8\ a_0$ and $E = 2$ eV).

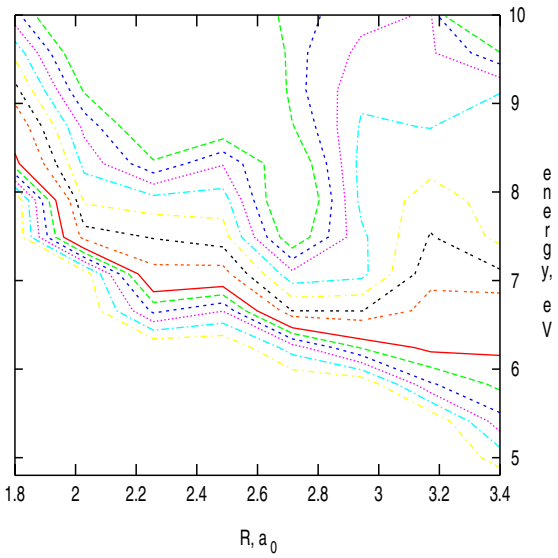

Figure 9. Contour plot of Born corrected total cross sections for electron impact excitation of the third excited $^2\Delta$ state plotted as a function of R. Contours range from $0.1\ a_0^2$ (bottom curve) to $1.4\ a_0^2$ (top contour) in steps of $0.1\ a_0^2$.

4. Conclusions

We have performed the first study of low-energy electron collisions with the CF molecule. The elastic cross section and the excitation cross sections for the five lowest-lying electronically

excited states of CF were calculated with the UK polyatomic *R*-matrix code (Morgan *et al* 1998), using a target model which gives a good agreement with theoretical and experimental data for the vertical excitation energies and the ground state dipole moment. We have developed a new approach for treating molecules with Rydberg states within the *R*-matrix method. The profile of the $^2\Sigma^+$ Rydberg state energy curve, derived using our model, shows good agreement with the larger MRCI calculations of Petsalakis (1999). Although target calculations performed using our new approach gave good results, the Rydberg orbital space used to construct Rydberg NO could probably be improved to give better target parameters over the whole range of *R* values.

Our calculations show the presence of three shape resonances of symmetries $^1\Delta$ and $^1\Sigma^+$ and $^3\Sigma^-$. These resonances are broad and short-lived. Performing calculations where the C–F bond was stretched from 1.8 to 3.6 a_0 we found that the $^3\Sigma^-$ and $^1\Delta$ resonances become bound at a bond length beyond 2.5 and 3.3 a_0 respectively, thus providing a route for dissociative electron attachment (DEA) for this molecule. The magnitude of the DEA cross section is estimated to be about 600 a_0^2 at 100 meV. Therefore, a substantial proportion of the CF radicals produced in any plasma reactor will undergo DEA above the surface of the etching wafer. Such negative ions can produce a plasma sheaf above the surface which affects the surface chemistry.

Although there are no experimental data on the cross sections for the CF molecule, previous studies on molecular radicals (Baluja *et al* 2001b) suggest that our elastic cross section should be reliable for energies above 100 meV. Below this energy rotational coupling needs to be explicitly included.

Acknowledgments

This work was supported by the British Government and the UK Engineering and Physical Sciences Research Council. We wish to thank to J D Gorfinkiel and Natalia Vinci for useful discussions. Most of the calculations were performed on the SUN cluster computer Ra at UCL Hiperspace computer centre.

References

Andrews E B and Barrow R F 1950 *Nature* **165** 890
Baluja K L, Mason N J, Morgan L A and Tennyson J 2000 *J. Phys. B: At. Mol. Opt. Phys.* **33** L677
Baluja K L, Mason N J, Morgan L A and Tennyson J 2001a *J. Phys. B: At. Mol. Opt. Phys.* **34** 2807
Baluja K L, Mason N J, Morgan L A and Tennyson J 2001b *J. Phys. B: At. Mol. Opt. Phys.* **34** 4041
Burke P G and Berrington K A 1993 *Atomic and Molecular Processes—an R-matrix Approach* (Bristol: Institute of Physics Publishing)
Byfleet C R, Carrington A and Russel D K 1971 *Mol. Phys.* **20** 271
Carrington A and Howard B J 1970 *Mol. Phys.* **18** 225
Carroll P K and Grennan T P 1970 *J. Phys. B: At. Mol. Phys.* **3** 865
Chu S I and Dalgarno A 1974 *Phys. Rev.* **10** 788
Cooper D L and Kirby K 1987 *J. Chem. Phys.* **87** 424
Dunning T H Jr, White W P, Pitzer R M and Mathews C W 1979 *J. Mol. Spectrosc.* **75** 297
Field D, Jones N C, Gingell J M, Mason N J, Lunt S L and Ziesel J-P 2000 *J. Phys. B: At. Mol. Opt. Phys.* **33** 1039
Grieman F J, Droege A T and Engelking P C 1983 *J. Chem. Phys.* **78** 2248
Hall J A and Richards W G 1972 *Mol. Phys.* **23** 331
Hess B A and Buenker R J 1986 *Chem. Phys.* **101** 211
Huber K P and Herzberg G 1979 *Constants of Diatomic Molecules* (New York: Van Nostrand-Reinhold)
Luque J, Hudson E A, Booth J-P and Petsalakis I D 2003 *J. Chem. Phys.* **118** 1206
Mason N J *et al* 2003 *Int. J. Mass Spectrom.* **223** 647–60
McLean A D and Yoshimine M 1967 *J. Chem. Phys.* **47** 3256

Morgan L A, Tennyson J and Gillan C J 1998 *Comput. Phys. Commun.* **114** 120
Petsalakis I D 1999 *J. Chem. Phys.* **110** 10730
Porter T L, Mann D E and Acquista N 1965 *J. Mol. Spectrosc.* **16** 228
Rendell A P, Bauschlicher C W and Langhoff S R 1989 *Chem. Phys. Lett.* **163** 354
Rozum I, Mason N J and Tennyson J 2002 *J. Phys. B: At. Mol. Opt. Phys.* **35** 1583
Saito S, Endo Y, Takami M and Hirota E 1983 *J. Chem. Phys.* **78** 116
Samukawa S, Mukai T and Noguchi 1999 *Mater. Sci. Semicond. Process.* **2** 203
Sarpal B K, Branchett S E, Tennyson J and Morgan L A 1991 *J. Phys. B: At. Mol. Opt. Phys.* **24** 3685
Tennyson J, Burke P G and Berrington K A 1987 *Comput. Phys. Commun.* **47** 207
Tennyson J and Morgan L A 1999 *Proc. R. Soc.* A **357** 1161
Tennyson J and Noble C J 1984 *Comput. Phys. Commun.* **33** 421